Translational Oncology 21 (2022) 101433

Contents lists available at ScienceDirect

Translational Oncology

journal homepage: www.elsevier.com/locate/tranon

Original Research

Eriodictyol mediated selective targeting of the TNFR1/FADD/TRADD axis in cancer cells induce apoptosis and inhibit tumor progression and metastasis

Shibjyoti Debnath [a], Abhisek Sarkar [a], Dipanwita Das Mukherjee [a], Subha Ray [a], Barun Mahata [a], Tarun Mahata [a], Pravat K. Parida [a], Troyee Das [b], Rupak Mukhopadhyay [c], Zhumur Ghosh [b], Kaushik Biswas [a,*]

[a] Division of Molecular Medicine, Bose Institute, Kolkata, West Bengal, 700054, India
[b] The Bioinformatics Center, Bose Institute, Kolkata, West Bengal, 700054, India
[c] Department of Molecular Biology & Biotechnology, Tezpur University, Assam 784028

ARTICLE INFO

Keywords:
Flavonoids
CRISPR-Cas9
Cell death
Tumorigenesis
Selective cytotoxicity

ABSTRACT

While the anti-inflammatory activities of Eriodictyol, a plant-derived flavonoid is well-known, reports on its anti-cancer efficacy and selective cytotoxicity in cancer cells are still emerging. However, little is known regarding its mechanism of selective anti-cancer activities. Here, we show the mechanism of selective cytotoxicity of Eriodictyol towards cancer cells compared to normal cells. Investigation reveals that Eriodictyol significantly upregulates TNFR1 expression in tumor cells (HeLa and SK-RC-45) while sparing the normal cells (HEK, NKE and WI-38), which display negligible TNFR1 expression, irrespective of the absence or presence of Eriodictyol. Further investigation of the molecular events reveal that Eriodictyol induces apoptosis through expression of the pro-apoptotic DISC components leading to activation of the caspase cascade. In addition, CRISPR-Cas9 mediated knockout of TNFR1 completely blocks apoptosis in HeLa cells in response to Eriodictyol, confirming that Eriodictyol induced cancer cell apoptosis is indeed TNFR1-dependent. Finally, *in vivo* data demonstrates that Eriodictyol not only impedes tumor growth and progression, but also inhibits metastasis in mice implanted with 4T1 breast cancer cells. Thus, our study has identified Eriodictyol as a compound with high selectivity towards cancer cells through TNFR1 and suggests that it can be further explored for its prospect in cancer therapeutics.

Introduction

Chemotherapy alone is seldom a feasible option owing to the development of chemoresistance, thereby, allowing tumor cells to escape drug action and resulting in cancer cell survival and treatment failure [1–3]. Hence, the need is to identify potential anti-cancer compounds, preferably from natural products, with novel modes of action that can selectively target the apoptotic machinery of the tumor cells without affecting the normal cells.

Some natural plant-based medications have limitations, such as adverse drug responses, toxicity, and safety, which restrict their therapeutic potential and necessitate improvement through medicinal chemistry [4–6]. Despite extensive testing of a wide range of natural plant-derived medicines, only a handful (such as Paclitaxel, Vinblastine,

Abbreviations: DISC, Death Inducing Signaling Complex; TNFR1, Tumor Necrosis Factor Receptor 1; FADD, FAS-Associated Death Domain Protein; TRADD, Tumor Necrosis Factor Receptor type 1-Associated DEATH Domain protein; CRISPR-Cas9, Clustered Regularly Interspaced Short Palindromic Repeats/CRISPR associated protein 9; RSK-2, Ribosomal S6 Kinase 2; ATF1, Activating Transcription Factor 1; NFkB, Nuclear Factor Kappa-light-chain-enhancer of activated B cells; TNF-α, Tumor Necrosis Factor-alpha(α); PARP1, Poly [ADP-Ribose] Polymerase 1; DMSO, Dimethylsulfoxide; FACS, Fluorescence Activated Cell Sorting; PE, Paired-End; PI, Propidium Iodide; PBS, Phosphate Buffer Saline; SDS-PAGE, Sodium Dodecyl Sulfate–Polyacrylamide Gel Electrophoresis; TBST, Tris Buffered Saline (Tween 20); PVDF, Polyvinylidene fluoride; ECL, Enhanced Chemiluminescence; OD, Optical Density; DTT, Dithiothreitol; MTT, 3-(4,5-dimethylthiazol-2-yl)-2,5-diphenyl tetrazolium bromide; IC_{50}, Half-maximal Inhibitory Concentration; CDK1, Cyclin-Dependent Kinase 1; IPA, Ingenuity Pathway Analysis; rh TNF, Recombinant human Tumor Necrosis Factor.

* Corresponding author.
E-mail address: kbiswas_1@yahoo.com (K. Biswas).

https://doi.org/10.1016/j.tranon.2022.101433
Received 22 October 2021; Received in revised form 11 April 2022; Accepted 11 April 2022

Camptothecin analogues, and others) have been approved for clinical use as potent anti-cancer chemotherapeutics [6]. However, due to the extensive biodiversity of the plants and numerous benefits of the plant-based natural agents (like the ease in availability, prominent efficacy, less toxicity, etc.), worldwide, they are under comprehensive research as promising scaffolds and leads for the development of more effective and selective anti-cancer agents for future therapeutic implication. Eriodictyol, a flavonoid is well-known for its anti-inflammatory and anti-oxidant properties [7]. Literature suggests that Eriodictyol abrogates RSK2-ATF1 signaling thereby inhibiting EGF-triggered neoplastic transformation [8] and inducing tumor cell apoptosis in combination with epigallocatechin-3-gallate [9]. It has also been shown to induce selective cytotoxicity in cancer cells over normal cells, although, the mechanism of its selectivity towards cancer cells is unclear and demands further research [10–12]. This lacuna led us to propose a detailed investigation of its precise molecular mechanism to delineate the cause for its high selectivity towards cancer cells.

The present study explores the contribution of the TNFR1-mediated death pathway in Eriodictyol-induced cytotoxicity in a panel of cancer cell lines, hand-in-hand with normal cells. Data from *in vitro* cell culture-based experiments clearly highlights a significant ability of Eriodictyol to selectively target cancer cell lines, with minimal effect on the normal cells, since it not only inhibits proliferation but also induces cancer cell apoptosis much more effectively than on normal cell lines. Eriodictyol-induced apoptosis is also characterized by an increase in membrane-associated TNFR1, which activates Caspase-8, followed by proteolytic inactivation of PARP1 via caspase-7 activation. Further, HeLa cells display significantly elevated levels of TNFR1 and also, dramatically upregulates the same in response to Eriodictyol, while, normal cells (HEK, NKE and WI-38) neither show any visible TNFR1 expression nor upregulate TNFR1 upon Eriodictyol treatment, thereby, explaining the plausible underlying selectivity of Eriodicytol's anti-cancer activity. An *in vivo* study in syngeneic mice (Balb/c) model implanted with the 4T1 breast cancer cells shows that Eriodictyol impedes tumor growth and metastatic progression with no sign of adverse effects on the animals. Therefore, we have highlighted Eriodictyol as a potent compound specifically targeting cancer cells of the cervical, breast, colon and renal origin and identified the mechanism behind its selective cytotoxicity in cancer cells compared to normal cells. Hence, this study supports the potentiality of Eriodictyol to be investigated as a promising chemotherapeutic agent.

Materials and methods

Reagents

Eriodictyol (#89061) was purchased from Merck, India. Primers were purchased from IDT, USA. Primary antibodies TRADD (#3994), FADD (#2782), TNFRI (#3736), Bax (#3994), Survivin (#2808), Claspin (#2800), γH2A.X (#80312), p21 (#2947), Caspase 7 (#9494), Caspase 8 (#9746), HSP90 (#4874), Cdc25A (#3652) and PARP1 (#9532) were obtained from Cell Signaling Technology (CST), USA. Bcl2 (sc-7382) was bought from Santa Cruz Biotechnologies (USA). Housekeeping genes β-actin (BB-AB0024) and GAPDH (BB-AB0060) were obtained from Biobharati Life Sciences Pvt. Ltd. (India). Cdc2 (ab 18), phospho-Cdc2 (Tyr15) (ab47594), Cyclin B1 (ab32053) primary antibodies and colorimetric assay kit of caspase 3 (ab39401) were obtained from Abcam, Cambridge, UK. Santa Cruz Biotechnologies provided the Z-VAD-FMK (sc3067). Gibco, USA provided FBS (#16000044), L-glutamine, gentamicin, sodium pyruvate and MEM non-essential amino acids.

Cell culture and maintenance

HeLa (Human Cervical cancer), HCT116 (Human Colon cancer) and WI-38 (Normal lung fibroblast) cell lines were originally obtained from ATCC (USA). Additionally, human cell lines, NKE (Normal kidney epithelial) and SK-RC-45 (Renal cancer cells), as well as murine tumor cell lines, 4T1 (Breast cancer), CT-26 (Colon cancer) and Renca (Renal cancer) were a kind gift from Dr. James H. Finke (Cleveland-Clinic, USA) and Dr. Gerd Ritter (Ludwig Institute of Cancer Research, USA) respectively. HEK (Human embryonic kidney) and MCF-7 (Human Breast cancer) cell lines was obtained from NCCS, Pune, India. The cell lines described above were grown in either RPMI 1640 or DMEM with 10% FBS and other supplements at 37 °C in presence of 5% CO_2 [13].

MTT cell proliferation assay

MTT assay was performed to determine the effect of Eriodictyol on cellular proliferation of normal and cancer cell lines. Briefly, cells were grown in 48 well plate formats in presence of Eriodictyol (0–200 μM) for 72 h. Phenol red-free RPMI without serum containing MTT (0.5 mg/mL; 200 μL per well) were added to each well and incubated at 37 °C for 3 h in a humidified incubator containing 5% CO_2. The purple-colored formazan crystals formed by cells were dissolved in DMSO and absorbance was measured at 570 nm in a microplate reader [14]. The selectivity index for human cancer cell lines SK-RC-45, HeLa, HCT-116 and MCF-7 was calculated from the ratio of their respective IC_{50} values and that of normal cell lines (WI-38 and NKE) [15].

Clonogenic survival assay

For clonogenicity assay, cells were plated at very low density (200 cells/well in 6 well plates), grown for either 8/10 days, fixed, and stained with 3.7% formaldehyde and 0.05% crystal violet. The assay provides a measure of the replicative capacity of the cells, which is dependent on the ability of the cells to form clones from a single cell. Images of wells containing cells were captured using Gel Doc XR+ (Bio-Rad). The method of quantification of the clones is mentioned in the respective legend [15].

Cell cycle profiling assay

For this experiment, HCT-116 cells were treated with increasing concentrations (100 μM, 150 μM, 200 μM) of Eriodictyol for 24 h, while HeLa cells were treated with 50 μM, 100 μM, 200 μM of Eriodictyol for 24 h. Post-treatment, cells were harvested into a single cell suspension and fixed by incubating the cells overnight at -20 °C with 75% ethanol. Cells were centrifuged and resuspended in 1 × PBS for 2 h followed by RNase A (20 μM) treatment for 2 h at 37 °C. Finally, cells were incubated with Propidium Iodide (PI) for 15 min at room temperature. Flow cytometric analysis was immediately performed using FACSuite™ software [15].

Annexin-V-FITC/PI staining

Briefly, post-treatment with Eriodictyol, 2×10^5 cells were washed with ice-cold 1X PBS and resuspended in 100 μL of 1X binding buffer. Cells were incubated with 5 μL of annexin-V-FITC followed by 5 μL of PI for 15 min at room temperature in a dark place as per the manufacturer's protocol. Finally, the percentage of stained cells was measured in the FACS-Verse instrument (BD) and analyzed using FACSuite™ software [16].

RNA sequencing data analysis

Total RNA was extracted using TRIzol reagent (Invitrogen) and purified by DNase treatment (ThermoFisher Scientific). The quality of the RNA samples was checked on Agilent TapeStation and quantified by Qubit fluorometer. The PE Illumina libraries were loaded onto NovaSeq6000 for cluster generation and sequencing. The trimmed reads were aligned with Human GENCODE hg38 reference genome using Hisat2

2.1.0. Following the sorting of Bam files with Samtools v1.19, transcripts assembly and differential gene analysis were performed with Cufflinks v2.2.2.1 and Cuffdiff v2.2.1, respectively, and differentially expressed genes with a fold change greater than equal to 2 and p and q value cut off of less than or equal to 0.05 were filtered out. Finally, gene enrichment and pathway analysis were performed with IPA (Ingenuity Pathway Analysis).

Western immunoblotting

Briefly, cell lysates were prepared from HeLa cells post-treatment with Eriodictyol (150 μM) using RIPA buffer. For immunoblotting, 30–50 μg proteins were resolved on 10–15% SDS-PAGE, transferred onto PVDF/nitrocellulose membrane (Millipore, USA), blocked with 5% BSA dissolved in 1X TBST, and subsequently probed with respective primary antibodies and secondary antibodies. Finally, blots were developed onto X-Ray films by the ECL method or by using gel imaging system (ChemiDoc MP, Bio-Rad and iBright Imager, Invitrogen) [13].

Caspase-3/7 activation assay

The assay was based on the ability of the enzyme(s) to detect and cleave the sequence DEVD from the chromophoric substrate DEVD-pNA. Caspase-3/7-dependent sequence specific cleavage of DEVD-pNA to release p-NA (p-nitro-aniline) from the substrate and its colorimetric detection enables quantitative measurement of the activity of Caspase-3/7 in the lysates. For this, cell lysates were prepared from HeLa using RIPA buffer following treatment with Eriodictyol. An aliquot of 150 μg of protein was used for each condition. DTT and DEVD-pNA substrate were added according to the manufacturer's (Abcam #ab30401) instructions. Samples were mixed well and incubated at 37°C for 90 min and finally, OD was measured at 405 nm in Multiskan GO microplate reader (ThermoFisher Scientific) [15].

Design, construction and validation of TNFR1 CRISPR

Guide oligos (20-mers) were designed from TNFR1 exon 2 sites using http://crispr.mit.edu (Supplementary figure S1A), on the basis of high "on-target score" and low "off-target score" in the whole exome. Guide oligo was then cloned into Cas9 expression vector (pSpCas9(BB)-2A-Puro) (Supplementary figure S1 B) having a puromycin selection cassette, sequence verified and TNFR1-CRISPR plasmid was transfected into HeLa cells using lipofectamine LTX reagent (Invitrogen) to check the functionality of the CRISPR plasmids within the cells. Following initial selection with puromycin (1mg/ml) over the week, genomic DNA was isolated from transfected cells and a mismatch heteroduplex sensing T7E1 assay was performed [17]. Next, clonal expansion from single cells was performed followed by immunoblotting of clonally expanded cells to screen for stable TNFR1-CRISPR knockout cells.

Real-time PCR and RNA isolation

Total RNA was extracted using TRIzol reagent (Invitrogen). 1 μg of RNA was extracted from HeLa cells treated with Eriodictyol along with DMSO-treated control. Verso cDNA synthesis kit (ThermoFisher Scientific) was used to convert RNA to cDNA. Real-Time PCR was performed in triplicate with a diluted stock of cDNA (1:6) mixed with SYBR green on Real Time PCR system 7500 Fast (Applied Biosystems) or QuantStudio 3 Real Time PCR system. Every mRNA quantification data were normalized to GAPDH and expressed as the fold differences of target gene expression relative to non-treated samples [18]. Primers used in this study are the following: TNFα: 5'-TGTAGCAAACCCTCAAGC-3' (forward), 5'- TGGGAGTAGATGAGGTACAG-3' (reverse); TNFR1: 5'-TTCGTCCC TGAGCCTTT-3' (forward), 5'- CAGGAGTGCCAAGTTTC-TAT-3' (reverse); GAPDH: 5'-ACAACTTTGGTATCGTGGAAGG-3' (forward), 5'-GCCATCACGCCACAGTTTC-3' (reverse).

4T1 breast tumor model

Female Balb/c mice aged 6–8 weeks were obtained from the Center for Translational Animal Research (CTAR) at the Bose Institute in Kolkata, India. The protocol was approved by the Bose Institute Animal Ethics Committee (Approval No. IAEC/BI/118/2018, dated 20/12/2018) and all animal experiments were performed in accordance with the institutional guidelines and in compliance with the CPCSEA regulations (based on NIH guidelines) based on the recommendations of the institutional animal ethics committee. 4T1 cells (1×10^6 cells/animal) were subcutaneously implanted into the mammary fat pad of Balb/c mice for the *in vivo* tumorigenic experiment. Following the formation of a palpable tumor, animals were randomly divided into two groups: vehicle control (5% DMSO) and Eriodictyol-treated (60 mg/kg), each consisting of at least five animals, and were subjected to intraperitoneal injections beginning around 10 days after tumor formation and lasting until 22 days (5 doses, 72 h interval). On every third day, the volume of the tumor was measured with vernier calipers using the equation Tumor volume $= 0.5 \times a \times b^2$, where "a" and "b" indicate major and minor axis, respectively.

4T1 tumor metastasis in secondary organs

4T1 tumor cells (1×10^5) were injected intravenously through the tail vein in syngeneic Balb/c mice. Post-inoculation, mice were randomly divided into three groups and administered with either 5% DMSO or two different doses of Eriodictyol, thrice a week. 3-4 weeks post-injection of tumor cells, animals were sacrificed and scrutinized for micro-metastatic nodule formation in the lungs, which is indicative of metastasis, and subjected to the counting of the number of micro-metastatic nodules as well as tissue staining of the lung cross-sections with hematoxylin-eosin (H&E).

Statistical analysis

Statistical analysis was performed by Student's t-test using GraphPad Prism 5.0 software. Statistical comparisons between groups were determined by a one-tailed or two-tailed Student's t test. The data are represented as mean ± SEM of at least three independent experiments, unless mentioned otherwise. The p values were used to ascertain if the values were statistically significant ($*p < 0.05$, $**p < 0.01$, $***p < 0.001$, ns = not significant). The statistical analysis of each experiment is detailed in the respective legends.

Results

Eriodictyol induces selective cytotoxicity to cancer cell lines

MTT cell viability assay indicates that Eriodictyol displays high toxicity towards human cancer cells SK-RC-45 (IC_{50}=53.75 μM), HeLa (IC_{50}=107.5 μM), HCT-116 (IC_{50}=105 μM) and MCF-7 (IC_{50}=75 μM) as well as murine cancer cells, 4T1 (IC_{50}=75 μM), CT-26 (IC_{50}=47.5 μM) and Renca (IC_{50}=145 μM) dose-dependently (Figs. 1A-1D). Interestingly, it is negligibly toxic towards normal human lines, NKE and WI-38 as indicated by IC_{50}>200 μM (Figs. 1E, 1F). The selectivity index (SI) measures a compound's cytotoxicity against cancer cells relative to non-tumor cells. The higher a compound's SI value, the more selective it is. The SI of Eriodictyol is calculated as the ratio of IC_{50} on normal cell line (NKE and WI-38) to the IC_{50} on cancer cell line (SK-RC-45 SI>3.72, HeLa SI>1.86, HCT116 SI>1.9, MCF-7 SI>2.66). The SI value of more than 1.5 has been considered as high selectivity. Therefore, this data not only demonstrates the selective cytotoxicity of Eriodictyol against different cancer cell lines over normal cells but also helps us in selecting the mouse tumor cell line for *in vivo* studies.

A

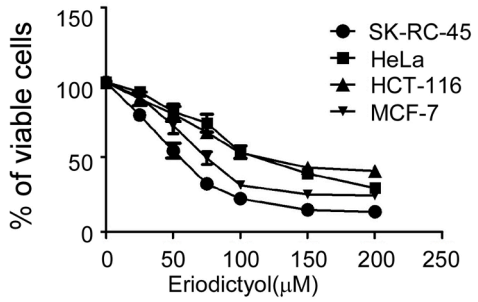

B

Human cancer cell lines	IC_{50} (μM)	Selectivity Index (SI)
SK-RC-45	53.75	>3.72
HeLa	107.5	>1.86
HCT-116	105	>1.90
MCF-7	75	>2.66

C

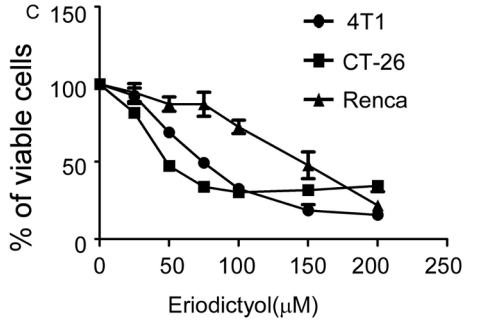

D

Mouse cancer cell lines	IC_{50} (μM)
4T1	75
CT-26	47.5
Renca	145

E

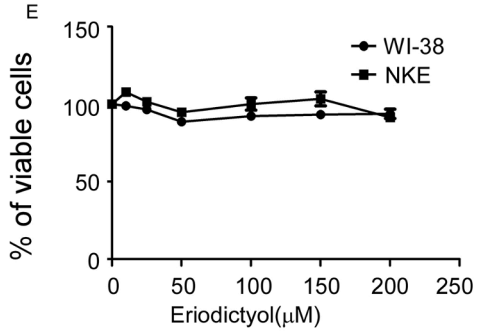

F

Human normal cell lines	IC_{50} (μM)
WI-38	>200
NKE	>200

G

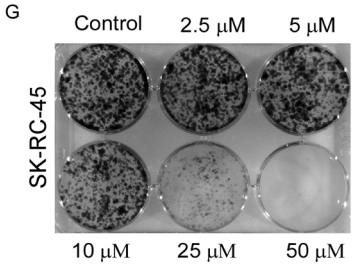

H

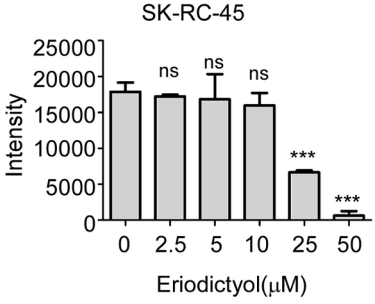

I

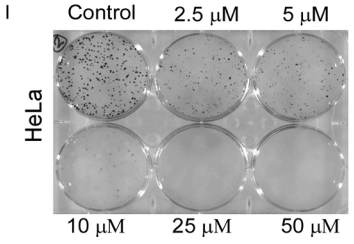

J

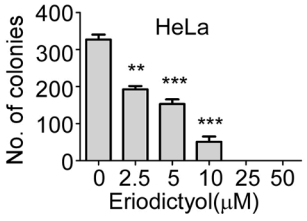

Fig. 1. Eriodictyol elicits selective cytotoxicity against several cancer cell lines. A, C, E. Line graphs showing in vitro cytotoxicity measured through MTT assay in presence of Eriodictyol (0-200 μM) at 72 h in human cancer (SK-RC-45, HeLa, HCT-116, MCF-7), mouse cancer (4T1, CT-26, Renca) and normal human (WI-38 and NKE) cell lines. The results are summarized from at least three independent experiments. **B.** Table depicting IC_{50} values and SI of human cancer cells. Selectivity index = mean IC_{50} ratio (normal cell line/cancer cell line). **D, F.** Displays the IC_{50} values of Eriodictyol in mouse cancer and normal human cell lines respectively. **G, I.** Pictorial representation of plates and **H, J**. Column graph showing dose-dependent inhibition of clonogenicity in SK-RC-45 (quantification of cell viability based on densitometry with image analysis by Bio-Rad ChemiDoc XRS) and HeLa cell lines (quantified by manual cell count) respectively, in response to Eriodictyol treatment. The results are shown as mean ± SEM of three independent experiments. Student's t-test were used for analysis (two-tailed;$^{*}p < 0.05$, $^{**}p < 0.01$, $^{***}p < 0.001$ vs non-treated, ns not significant).

Eriodictyol blocks clonogenicity of cancer cells

The ability of a single cell to form clones, as represented by clonogenicity, is a defining characteristic of cancer cells. Eriodictyol inhibits clonogenicity of SK-RC-45 cells at concentrations as low as 10 μM with a significant reduction in colony formation at 25 μM of Eriodictyol (Figs. 1G, H). Moreover, it shows better efficacy in HeLa cells with inhibition of clonogenicity starting from 2.5 μM with an almost complete regression of colony formation at 10 μM (Figs. 1I, J). It is clearly evident from the data, that while Eriodictyol significantly inhibits colony growth at a concentration as low as 2.5 μM in the case of HeLa cells, and 25μM in SK-RC-45 cells (Figs. 1G-J), the concentration of Eriodictyol that causes ~ 40–50% cells to undergo apoptosis at least in the case of HeLa and MCF-7 cells is 125 μM (Figs. 2A,B), which is evidently several folds higher than that required to inhibit significant clonogenicity. Therefore, we conclude that Eriodictyol effectively inhibits the clonogenicity of cancer cells.

Eriodictyol induces apoptosis in human and murine cancer cells

Apoptosis is characterized by the translocation of the phosphatidylserine (PS) from the cytosol to the cell membrane, which is experimentally detected by binding of annexin V-FITC to PS. Our flow cytometry study reveals that Eriodictyol treatment for 48 hours causes dose-dependent activation of apoptosis in HeLa and MCF-7 cells, as evidenced by a dose-dependent increase in the percentage of annexin-V +ve cell populations (Figs. 2A, B), while it caused only moderate, yet significant induction of apoptosis in HCT-116 cells (Fig. 2C). Similarly, Eriodictyol also induces apoptosis in mouse tumor cells, 4T1 and CT-26 (Figs. 2D, E), as indicated by a dose-dependent increase in the percentage of annexin-V +ve cells. Interestingly, a comparative study of the apoptosis induction between cancer cell lines, HeLa vs normal cell lines, WI-38 and NKE confirms that Eriodictyol induces a significantly higher level of apoptosis in the cancer cell line, HeLa as compared to both the normal cells, WI38 and NKE. However, while Eriodictyol elicits only a negligible level of apoptosis in WI-38 cells, NKE cells display only a moderate level of apoptosis in response to Eriodictyol treatment, and that too from 125 μM (Fig. 3). Collectively, these results confirm that the selective cytotoxicity of Eriodictyol not only resides in its ability to inhibit cancer cell proliferation but also, in inducing differential apoptosis in different cancer cell lines.

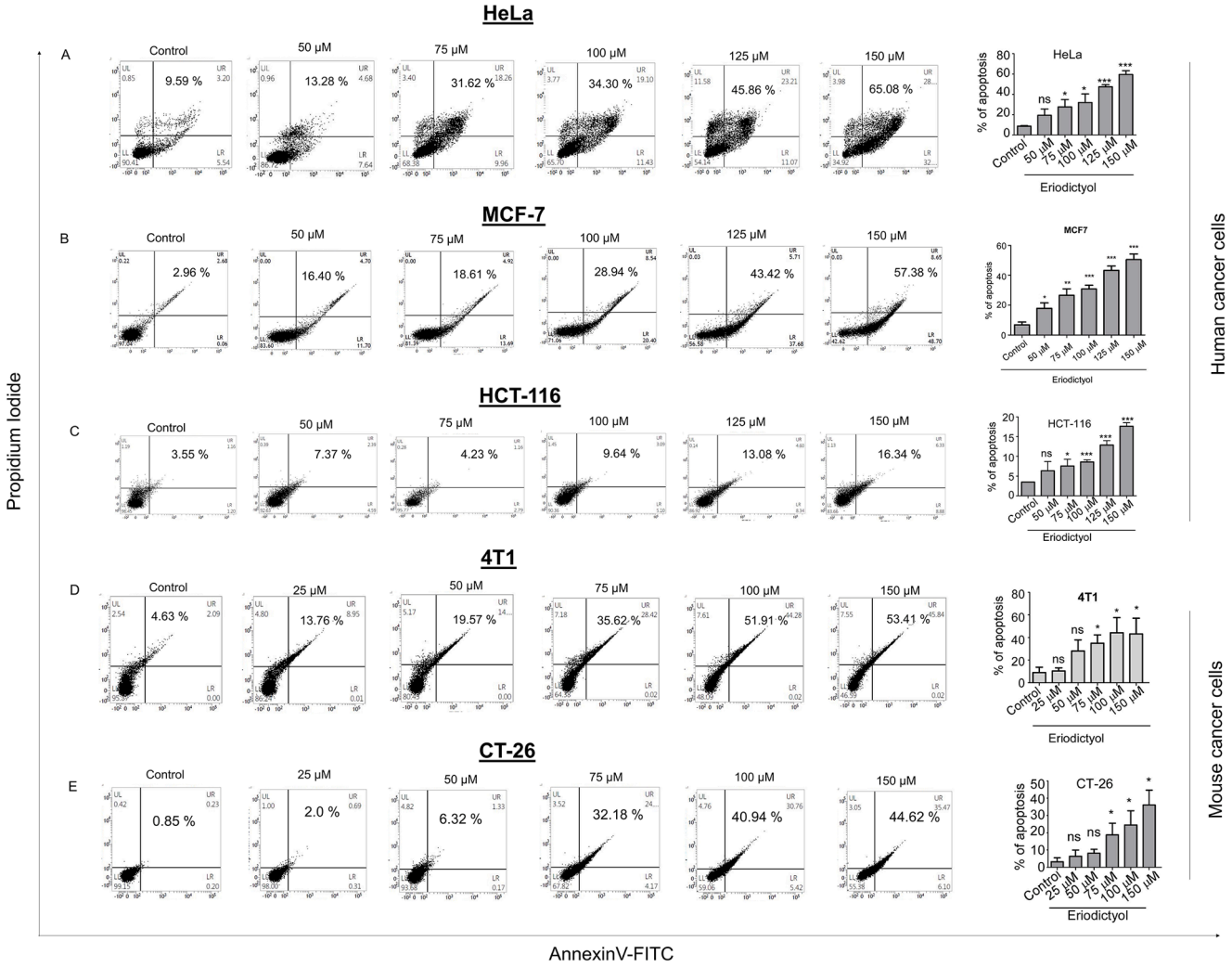

Fig. 2. Eriodictyol treatment induces apoptosis in human and mouse cancer cell lines. Flow cytometric density plots demonstrating a dose-dependent increase in the annexin V-FITC/PI-positive population of (A) HeLa, (B) MCF-7, (C) HCT-116, (D) 4T1, and (E) CT-26 cells in response to Eriodictyol treatment. Post-treatment with Eriodictyol (0–150 μM) for 48 h, cells were stained with annexin V-FITC/PI, apoptosis was measured in BD FACS Verse instrument and analyzed in BD FACSuite™. Data represent at least three independent experiments. Column graphs represent concentration-dependent induction of apoptosis in the above-mentioned cell types and experimental conditions. The data are represented as Mean ± SEM of three independent experiments and analyzed by Student's t-test (two-tailed); $*p < 0.05$, $**p < 0.01$, $***p < 0.001$, ns not significant. The total apoptosis population was calculated by combining the quadrants UL+UR+LR.

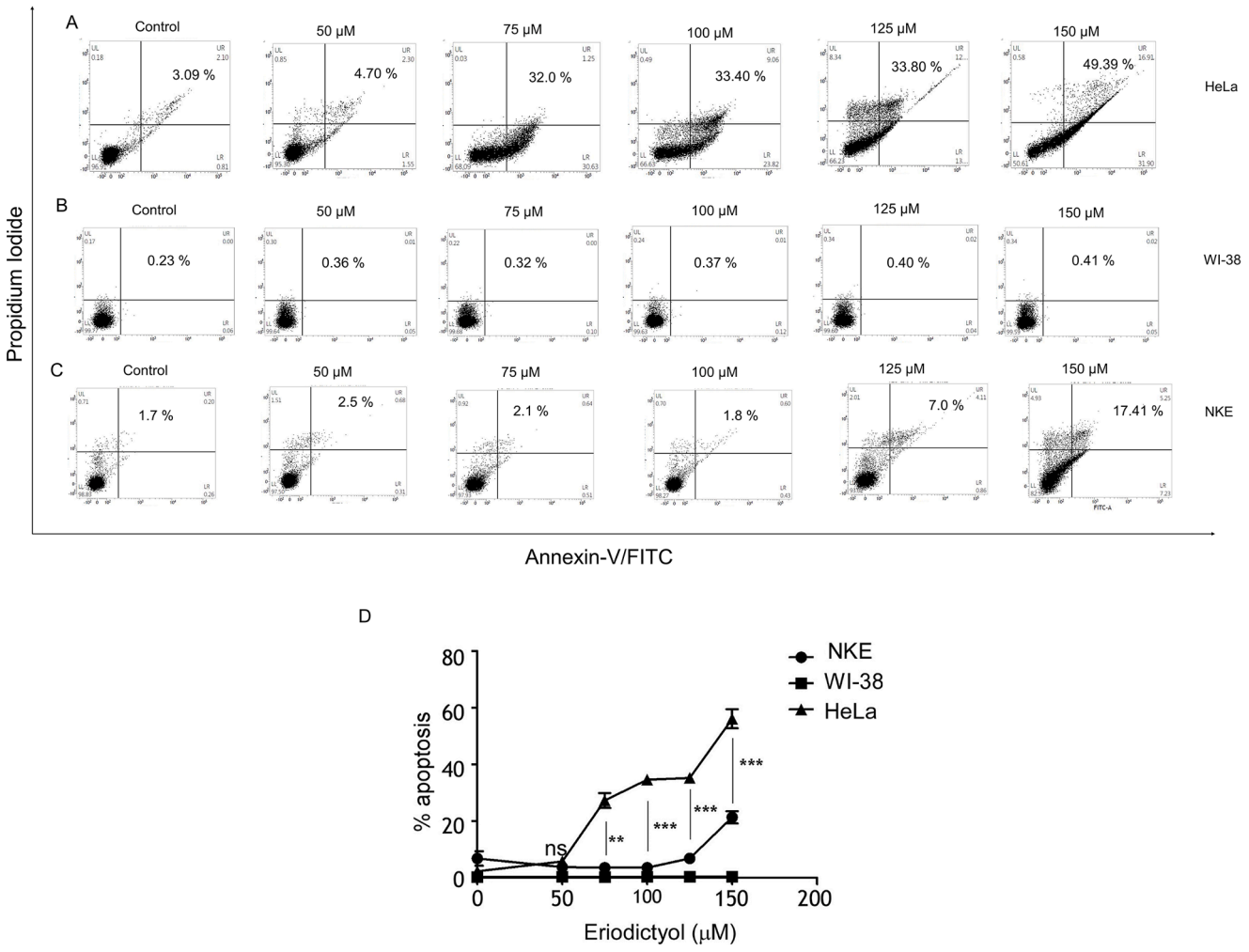

Fig. 3. Eriodictyol induced apoptosis in HeLa cells is significantly higher than that of WI-38 and NKE cells. Density plots showing comparative concentration-dependent induction of apoptosis in **(A)** HeLa versus normal **(B)** WI-38 and **(C)** NKE cell lines upon Eriodictyol treatment. **D.** Line graph representing the difference in the percentage of apoptosis in cancer cells compared to normal cell lines. The data are represented as Mean ± SEM of three independent experiments and analyzed by Student's t-test (two-tailed); $*p < 0.05$, $**p < 0.01$, $***p < 0.001$, ns not significant.

Eriodictyol arrests cell cycle progression at the G2/M phase

Flow cytometric determination of the cell cycle distribution of PI-stained cervical cancer and colon cancer cells indicates dose-dependent accumulation of HeLa (Figs. 4A, B) and HCT-116 (Figs. 4C-E) at the G2/M phase of the cell cycle upon Eriodictyol treatment. The activation of Cdc2 (CDK1) through dephosphorylation of Cdc2 at Thr14 and Tyr15 by a group of phosphatases e.g., Cdc25 has been reported as a critical regulatory step in the progression of cells to mitosis [19]. As evident from the Western blot (Fig. 4E), Eriodictyol causes a time-dependent increase in phosphorylation of Cdc2 at Tyr15, in addition, to a decrease in expression of Cdc2, Cdc25A indicating de-activation of Cdc2 , consequently leading to a delay in cell cycle progression to mitosis and holding the cells at the G2/M checkpoint.

Inhibition of Cdc2 by Eriodictyol results in the accumulation of cells in the G2 phase without mitosis, thus, resulting in the accumulation of Cyclin B1.

Eriodictyol stimulation induces differential expression of distinct gene sets implicated in proliferation, cell-cycle and apoptosis-related pathways in the HeLa cell line

To explore the extent of Eriodictyol mediated modulation of gene expression and associated biological processes, transcriptome sequencing is performed in Eriodictyol-treated versus non-treated cells at both early (6 h) and late (24 h) time points in HeLa cells. The primary analysis of the data on the Differentially Regulated Gene sets (DRGs) show distinctly different clustering of gene sets as evidenced from the heat map (Fig. 5A) in Eriodictyol treated versus non-treated cells. The transcripts with fold change (FC) $\geq$2 with p-value $\leq$0.05 are selected for our analysis. The volcano plot depicts a marked increase in the number of upregulated (apoptosis inducers and tumor suppressors) and down-regulated (metastasis inducers and cell cycle regulators) genes (Fig. 5B). Gene enrichment and pathway analysis have been performed with IPA (Ingenuity Pathway Analysis) and the results are grouped into three clusters (metastasis, apoptosis, and cell cycle) and represented as Venn diagram (Fig. 5C). Moreover, we have established a heat map displaying common tumor-related genes mostly affected by Eriodictyol (Fig. 5D), which displays a distinctly different gene expression profiling in the Eriodictyol treated versus non-treated cells. Data clearly shows distinct upregulation of apoptosis inducers and tumor suppressors and a significant decrease in oncogenes and cell cycle regulators in response to Eriodictyol. Finally, significant modulation of key biological processes in response to Eriodictyol treatment, many of which are closely related to or involved in apoptosis, metastasis and cell cycle regulation are represented as bar diagram (Fig. 5E). The results of canonical pathway analysis indicate that Eriodictyol may be involved in cell cycle regulation, specifically at the G2/M phase. In addition, pathway analysis

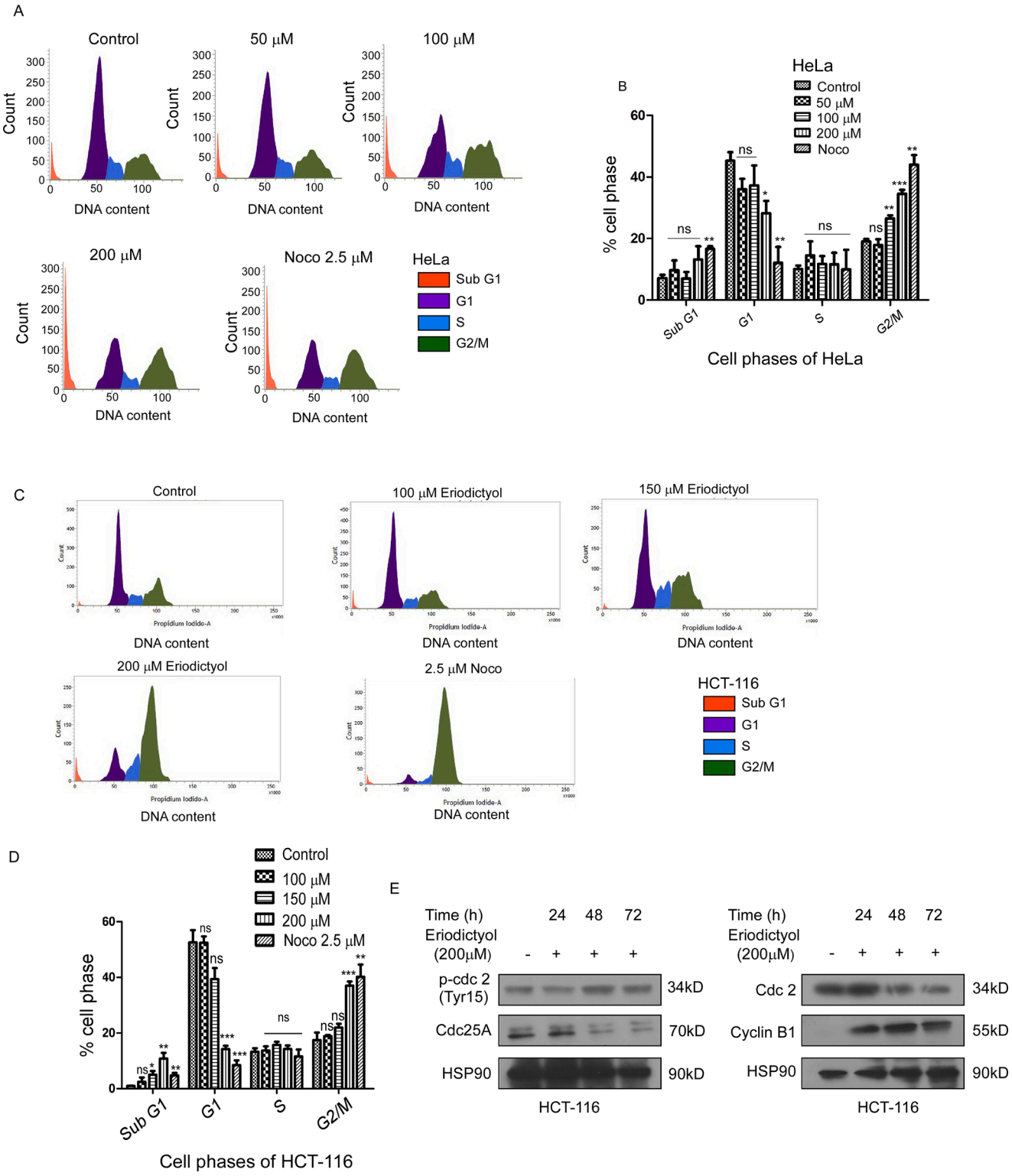

Fig. 4. Eriodictyol disrupts cell cycle progression by causing G2/M arrest. A. Histogram represents a dose-dependent increase in the G2/M phase population of Eriodictyol treated HeLa cells compared to untreated control cells for 24 h. **B.** Bar graph represents the percentage of HeLa cells at various phases of the cell cycle in response to Eriodictyol treatment. **C.** Histogram showing a dose-dependent increase in G2/M population and a corresponding decrease in G1 phase population in HCT-116 at 24 h post-treatment of Eriodictyol. **D.** Column graph depicting % of HCT-116 cells residing in various phases of the cell cycle in response to corresponding concentrations (0–200 μM) of Eriodictyol. Data represents Mean ± SEM of three independent experiments and Student's t-test (two-tailed;*$p < 0.05$, **$p < 0.01$, ***$p < 0.001$, ns not significant) was used for significance analysis. **E.** Western Immunoblots showing G2/M phase Cyclins and CDK protein expression at various time points (0–72 h) in response to Eriodictyol treatment. HSP90 was used as the loading control.

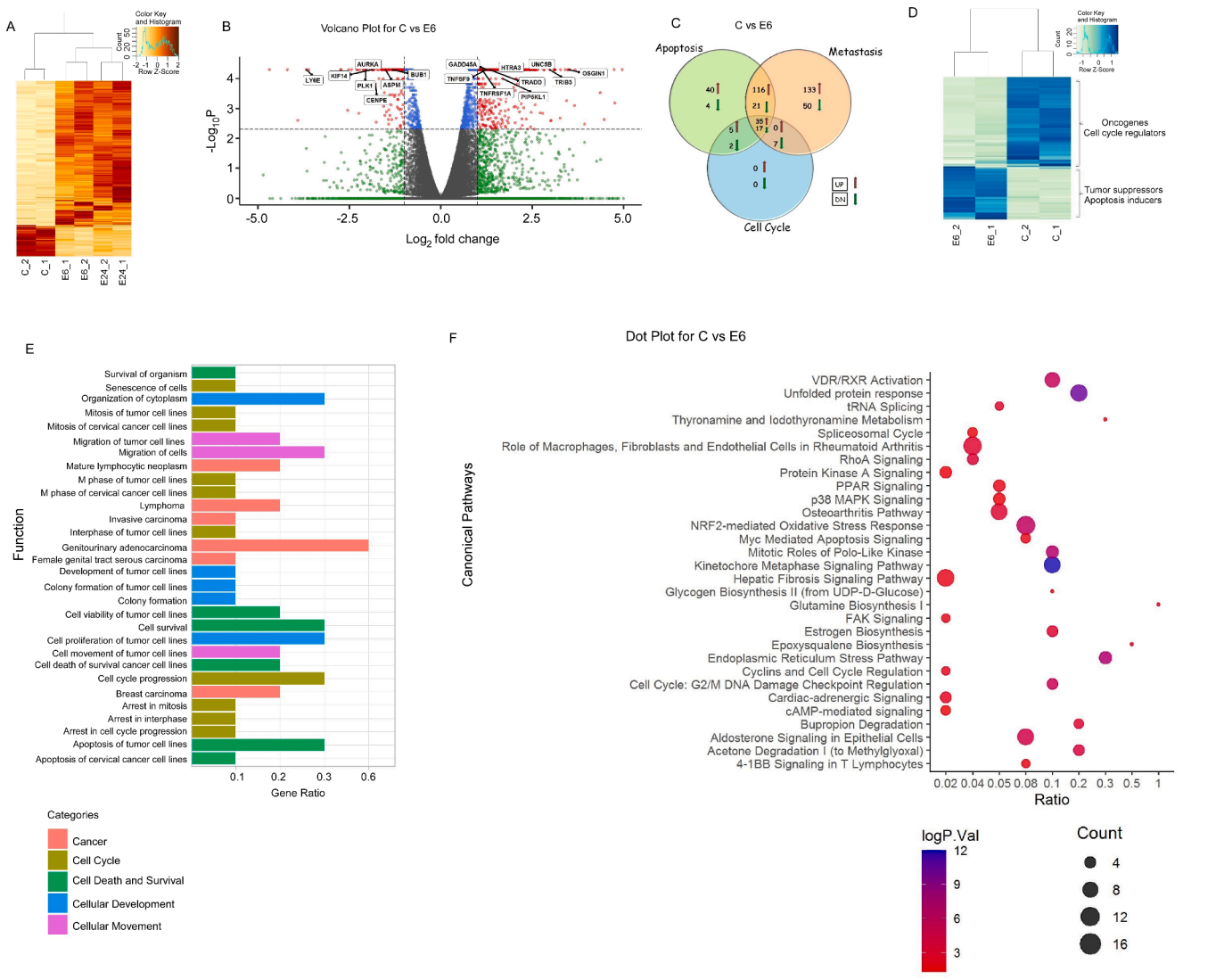

Fig. 5. Eriodictyol treatment induces differential expression of distinct gene sets implicated in apoptosis, metastasis, cell-cycle regulatory genes, and associated pathways in HeLa cells. A. A heat map showing differential regulation of global genes in response to Eriodictyol treatment in both 6 h (E6_1, E6_2) and 24 h (E24_1, E24_2) in comparison to untreated control (C_1, C_2). **B.** Volcano plot depicting the differentially regulated global genes at 6 h post treatment of Eriodictyol. **C.** Venn diagram analysis exhibiting total number of apoptosis, metastasis and cell cycle regulatory genes at 6 h Eriodictyol treatment. **D.** Heat map displaying a screened set of genes highly affected by Eriodictyol at 6 h through IPA analysis. **E.** Functional analysis represented as bar plot C vs E6. **F.** Ingenuity Pathway Analysis. The color intensity of the nodes shows the degree of enrichment of this analysis. The enrich-factor is defined as the ratio of the differential genes in the entire genome. The dot size represents the count of genes in a pathway. C_1- Untreated sample 1, C_2- Untreated sample 2, E6_1 - Treated sample 6 h sample 1, E6_2 - Treated sample 6 h sample 2, E24_1 - Treated sample 24 h sample 1, E24_2 - Treated sample 24 h sample 2.

reflects several pathways that are involved in the regulation of Cell Cycle, DNA-damage as well as Apoptotic responses, some of which are represented in Fig. 5F. Interestingly, TNFR1 is one of the genes that is not only significantly upregulated but also commonly involved in several of these pathways. Taken together, Eriodictyol causes differential regulation of gene expression that translates into the induction of apoptosis, cell cycle arrest and cytotoxicity to the tumor cells.

Eriodictyol disrupts pro-apoptotic/anti-apoptotic signal balance in cancer cells

Investigation of the detailed molecular events indicate the involvement of the DISC complex in Eriodictyol mediated apoptosis of HeLa cells, as evident from significant time-dependent upregulation in expression of the pro-apoptotic DISC components, i.e., TNFR1, FADD and TRADD (Fig. 6A).

In addition, Eriodictyol causes significant time-dependent increase of pro-apoptotic Bax, with a dramatic time-dependent decrease in anti-apoptotic Bcl2 and Survivin (Fig. 6B), thereby tipping the balance towards a pro-apoptotic outcome. Eriodictyol also causes time-dependent downregulation in the expression of the key anti-apoptotic and DNA-damage response protein, p21 in HeLa cells (Fig. 6C).

Furthermore, Eriodictyol treatment results in a time-dependent increase in the expression of the DNA fragmentation marker, γ-H2A.X, indicating that Eriodictyol may have a DNA damaging effect in cancer cells, perhaps leading to the activation of downstream apoptotic processes (Fig. 6C). Eriodictyol-mediated apoptotic cascade involves caspases as evident by a time-dependent reduction in pro-caspase 7 expression and an increase in cleaved caspase 7, activation of caspase 8, as well as a decrease in full-length 116 kDa PARP1 levels and the presence of the cleaved 89 kDa form (c-PARP1) (Fig. 6D). As shown in Fig. 6G, the caspase activity assay also confirms activation of caspase 3/7 in HeLa cells at later time points (24, 48 and 72 h). Pretreatment of HeLa cells with 20 μM inhibitor of PAN-caspase (Z-VAD-FMK) provide a

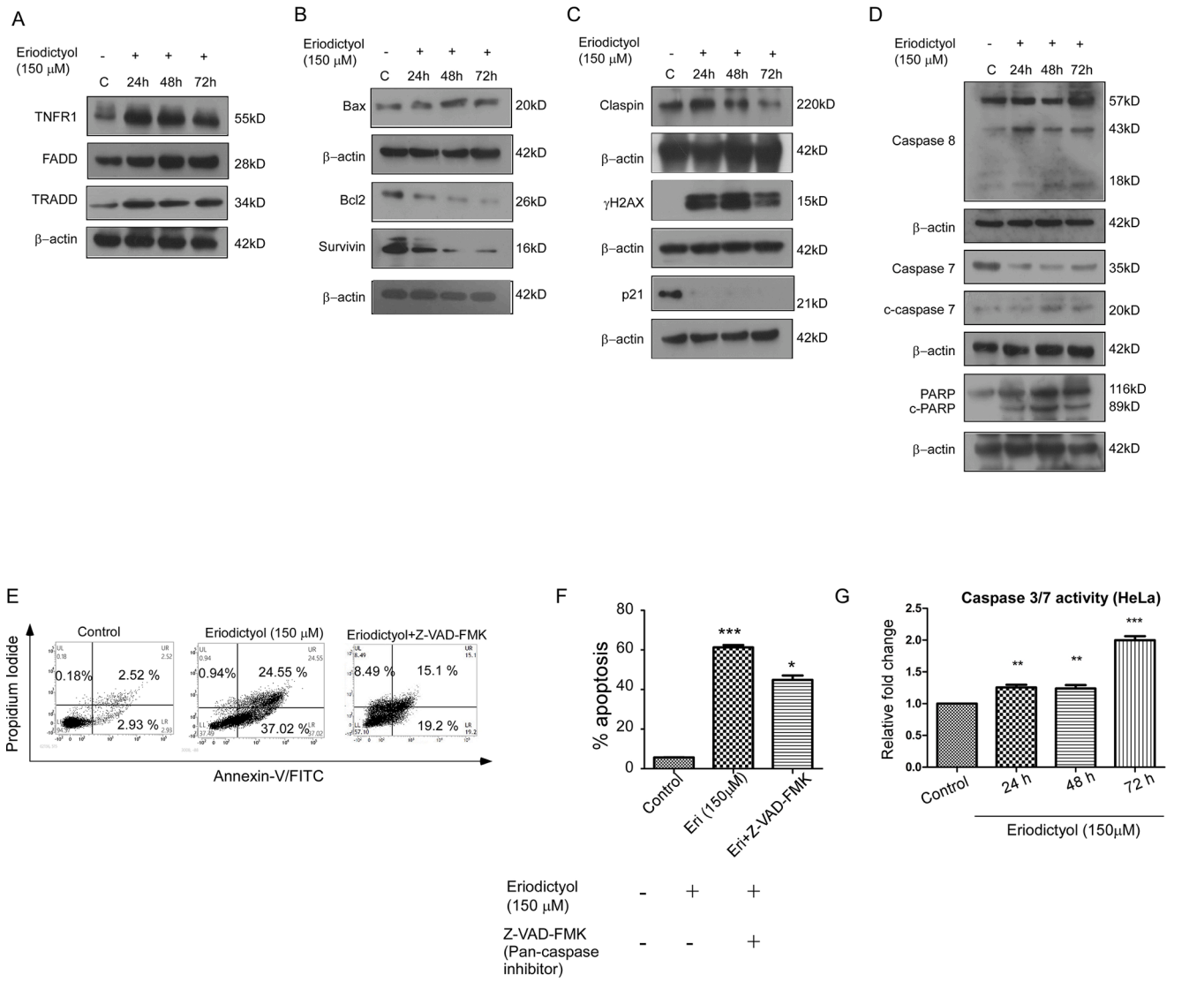

Fig. 6. Cancer cell apoptosis induced by Eriodictyol involves extrinsic pathway. A. Western immunoblots depicting increase in the expression levels of TNFR1, FADD and TRADD in HeLa cells upon Eriodictyol treatment. **B.** Eriodictyol treatment increases the expression of Bax and decreases the expression of Bcl2 and Survivin time dependently. **C.** Western immunoblots showing activation of DNA damage responsive protein expression in HeLa upon Eriodictyol treatment. **D.** Activation of the caspase cascade and PARP1 cleavage in HeLa cells upon Eriodictyol treatment. **E, F.** Density plot and column graph from flow cytometry analysis (BD FACSuite^{TM}) showing Eriodictyol mediated apoptosis in presence of pan-caspase inhibitor (Z-VAD-FMK) at 20 μM concentration, indicating that Eriodictyol mediated apoptosis is partially caspase dependent. **G.** Caspase 3/7 activity in response to Eriodictyol treatment at 24, 48, and 72 h is depicted in a column graph. Data represent Mean ± SEM of three independent experiments, analyzed by Student's t-test (two-tailed); $*p < 0.05$, $**p < 0.01$, $***p < 0.001$, ns not significant.

moderate (~ 31% inhibition), yet significant protection against Eriodictyol-mediated apoptosis (Figs. 6E, F), confirming that Eriodictyol mediated tumor cell apoptosis is at least partially caspases-dependent. Thus, collectively we confirm that Eriodictyol upregulates the pro-apoptotic proteomes and causes a significant reduction in survival proteins, thereby, culminating in a pro-apoptotic outcome in cancer cells.

TNFR1 is the potential target of Eriodictyol and the primary basis behind its selective cytotoxicity

Our preliminary data indicate that Eriodictyol treatment remarkably increases the mRNA levels of both TNF-α and TNFR1 in a time-dependent manner (Figs. 7A, B). Further, both the mRNA and protein levels of TNFR1 are elevated in HeLa cells, post-Eriodictyol treatment at 150 μM (Figs. 7 B, C). Multiple studies have reported that TNFR1 is involved in the extrinsic pathway of apoptosis [20]. To further elucidate the relationship between the selectivity of Eriodictyol towards cancer cells over normal cells, the basal expression level of TNFR1 is checked in non-cancerous cells (HEK, NKE and WI-38) versus cancer (SK-RC-45 and HeLa) cells. Western blot results clearly show that the basal level of TNFR1 protein expression in cancer cells is significantly higher than that in normal cells (Fig. 7D), thereby indicating that lack of expression of TNFR1 receptor in normal cells may be the reason for the observed selective activity of Eriodictyol against the cancer cells.

To further confirm, whether Eriodictyol selectively induces TNFR1 expression, the relative expression of Eriodictyol induced TNFR1 was checked in both cancers as well as normal cells. As shown in Fig. 7E, 24 h and 48 h exposure to Eriodictyol results in a significantly elevated time-dependent induction in TNFR1 expression in cancer (SK-RC-45 and HeLa) cells, while in the normal NKE and HEK cells, induction of TNFR1 expression with time is significantly lower compared to the cancer cells. Hence, this data supports the rationale for Eriodictyol's selective cytotoxicity towards cancer cells. Furthermore, remarkable dose-dependent upregulation in the induction of TNFR1 expression in HeLa cells initiates at 100 μM concentration of Eriodictyol compared to negligible or no TNFR1 expression in NKE (Fig. 7F, top panel) and WI-38 cells (Fig. 7F,

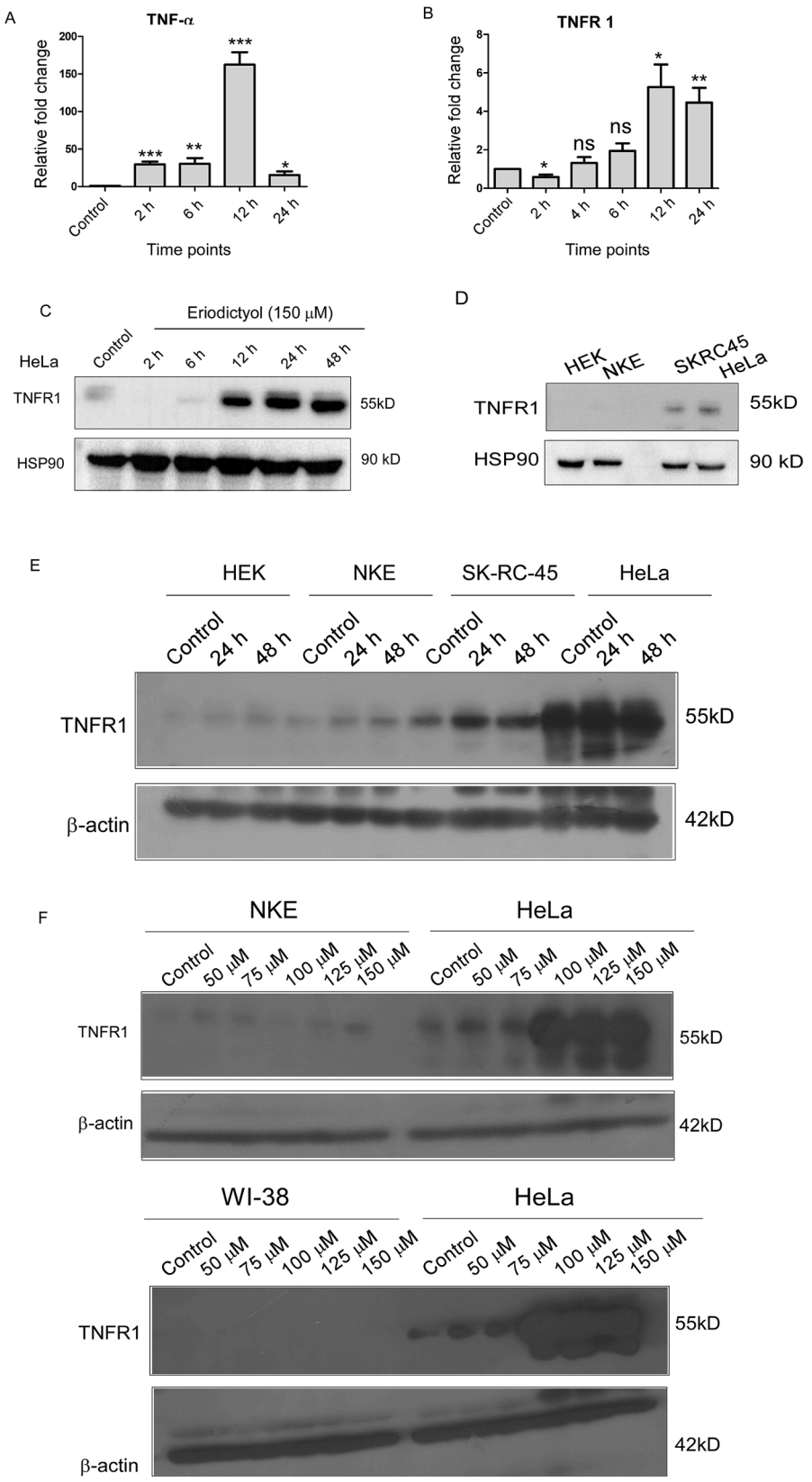

Fig. 7. Eriodictyol selectively activates TNFR1 in cancer cells but not in normal cells. A, B. Real time PCR reflecting time-dependent relative fold change in mRNA expression of TNF-α and TNFR1 respectively in response to Eriodictyol (150 μM). Relative expression values of target genes were normalized to their corresponding GAPDH Ct value and represented as fold change with respect to untreated control. Data represent mean ± SEM of three independent experiments (Student's t-test (two-tailed); $*p < 0.05$, $**p < 0.01$, $***p < 0.001$, ns-not significant). **C.** Western immunoblot data showing time-dependent induction in TNFR1 expression in HeLa cells upon Eriodictyol (150 μM) treatment. **D.** Western immunoblot confirming the basal expression level of TNFR1 in cancer lines (SK-RC-45 and HeLa) compared to normal cells (HEK and NKE). **E.** Western immunoblot showing comparative time-dependent (0h, 24h, 48h) induction of TNFR1 expression between cancer cells (SK-RC-45 and HeLa) and normal cells (HEK and NKE) in response to Eriodictyol (150 μM) treatment. **F.** Comparison of TNFR1 expression in NKE vs HeLa (Top panel) and WI-38 vs HeLa (Bottom panel) in response to various doses of Eriodictyol.

bottom panel), respectively, which correlates with the respective dose-dependent apoptotic window in HeLa cells (Fig. 3C).

Finally, to confirm the direct role of TNFR1 in the regulation of Eriodictyol mediated apoptosis, we have established TNFR1-knockout cells using CRISPR-Cas9 genome editing technology (Figs. 8A-C; Supplementary figure S1). Out of the 10 clones screened for the expression levels of TNFR1, 4 clones (Fig. 8A) appear to have complete depletion of TNFR1 expression. TNFR1 KO clone#6 is used for subsequent studies. While Eriodictyol induces significant apoptosis in wild type HeLa cells (>45% annexin V/PI + cells) at 150 μM, there is a

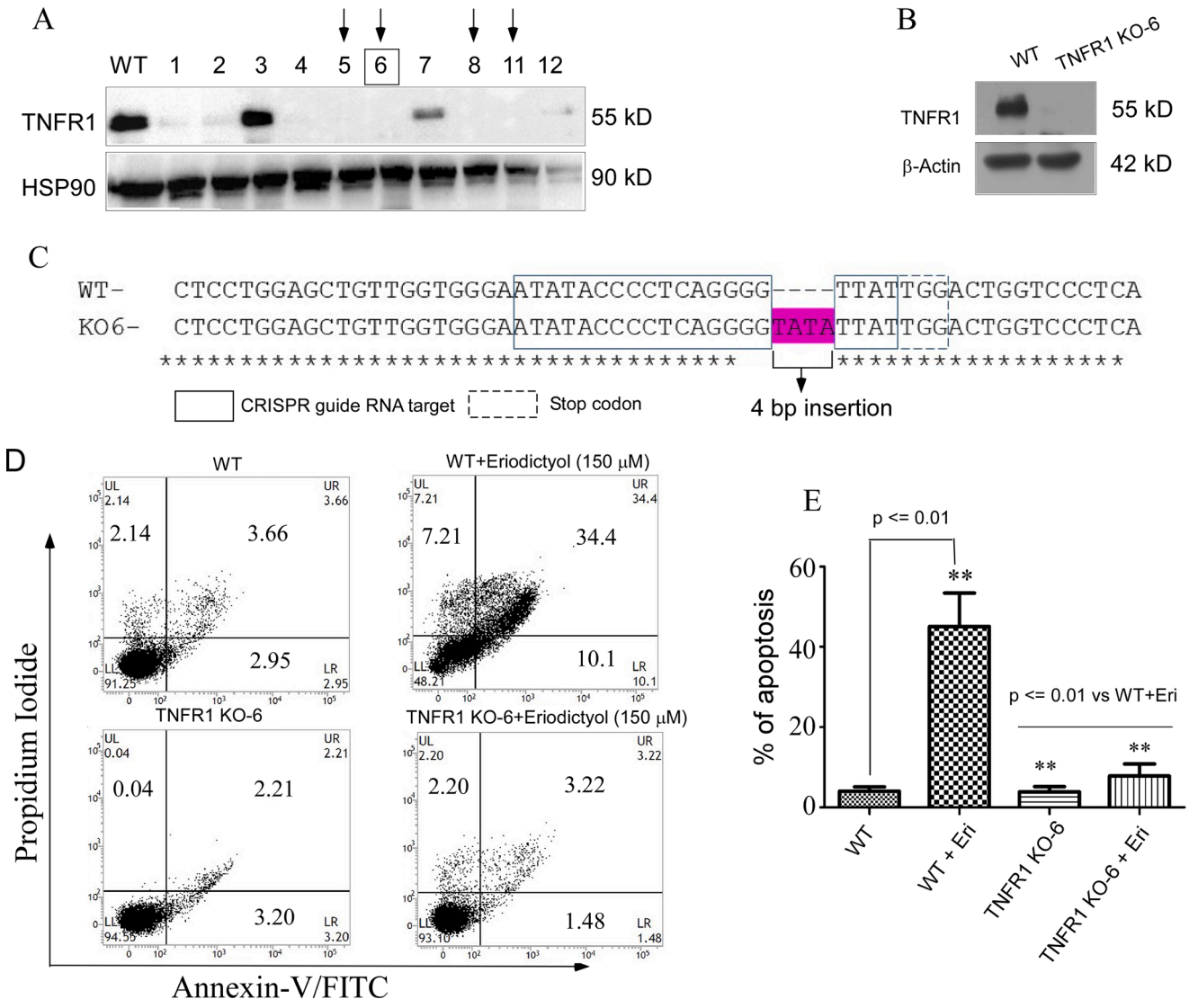

Fig. 8. CRISPR-Cas9 mediated knockout of TNFR1 in HeLa cells resulted in abrogation of Eriodictyol mediated apoptosis. A. Western immunoblot-based screening and selection of TNFR1 negative clones from an array of clones selected by puromycin treatment (1mg/ml). **B.** Western immunoblot showing TNFR1 expression in HeLa (wild-type) versus TNFR1 KO-6 clone. **C.** TNFR1 KO-6 clone shows 4bp insertion (TATA) that results in non-functional protein production. Inserted bases highlighted. The boxed portion represents the targeted DNA sequence. **D, E.** Density plot and bar graph from FACs analysis showing significant abrogation of apoptosis in TNFR1 KO-6 clone compared to HeLa (wild-type) upon Eriodictyol treatment at 150 μM dose for 48 h. Data has been collected from three independent experiments and analyzed by Student's t-test (two-tailed).

marked decrease in apoptosis in TNFR1 knockout clone KO-6 (~7% annexin-V/PI + cells) as evident from the density plot and bar graph (Figs. 8D, E), thereby confirming that Eriodictyol mediated tumor cell apoptosis is TNFR1-dependent. Therefore, we conclude that the TNFR1 signaling axis is important in the Eriodictyol-induced apoptosis of cancer cells.

Eriodictyol inhibits tumor development, progression and metastasis in immuno-competent mice

To translate the *in vitro* anticancer activity of Eriodictyol *in vivo*, a syngeneic mouse (Balb/c) tumor model has been used. *In vivo* findings demonstrate a substantial suppression of tumor development, as evident by a time-dependent decrease in tumor volume (Figs. 9A, B), as well as a decrease in the volume and weight of resected tumors from Eriodictyol-treated mice compared to non-treated animals (Figs. 9C, D). Eriodictyol-treated mice show no signs of toxicity as evident from the measurement of body weight of mice (Fig. 9E).

Moreover, Eriodictyol treatment results in a dose-dependent decrease in the number of lung metastatic nodules, (Figs. 9F, G) and a significant decline in the weight of the lungs in Eriodictyol –treated groups compared to the control group (Supplementary figure S2B). In summary, our *in vivo* study indicates that Eriodictyol reduces tumor growth and progression, as well as suppresses pulmonary lung metastasis of 4T1 cells in immune-competent Balb/c mice.

Discussion

One of the hallmarks of tumor cells is the evasion of apoptosis [21, 22]. Enhancement of the pro-apoptotic ability of the anti-cancer agents through abrogation of the survival signaling has been recognized as an effective strategy towards sensitizing the cancer cells to the chemotherapeutic drugs and preventing chemoresistance [23–25]. Owing to the increasing significance of the TNF pathway in cancer, the primary aim of the present study is to discover an effective TNF-mediated anti-cancer therapeutic with minimal toxicity to the normal cells and

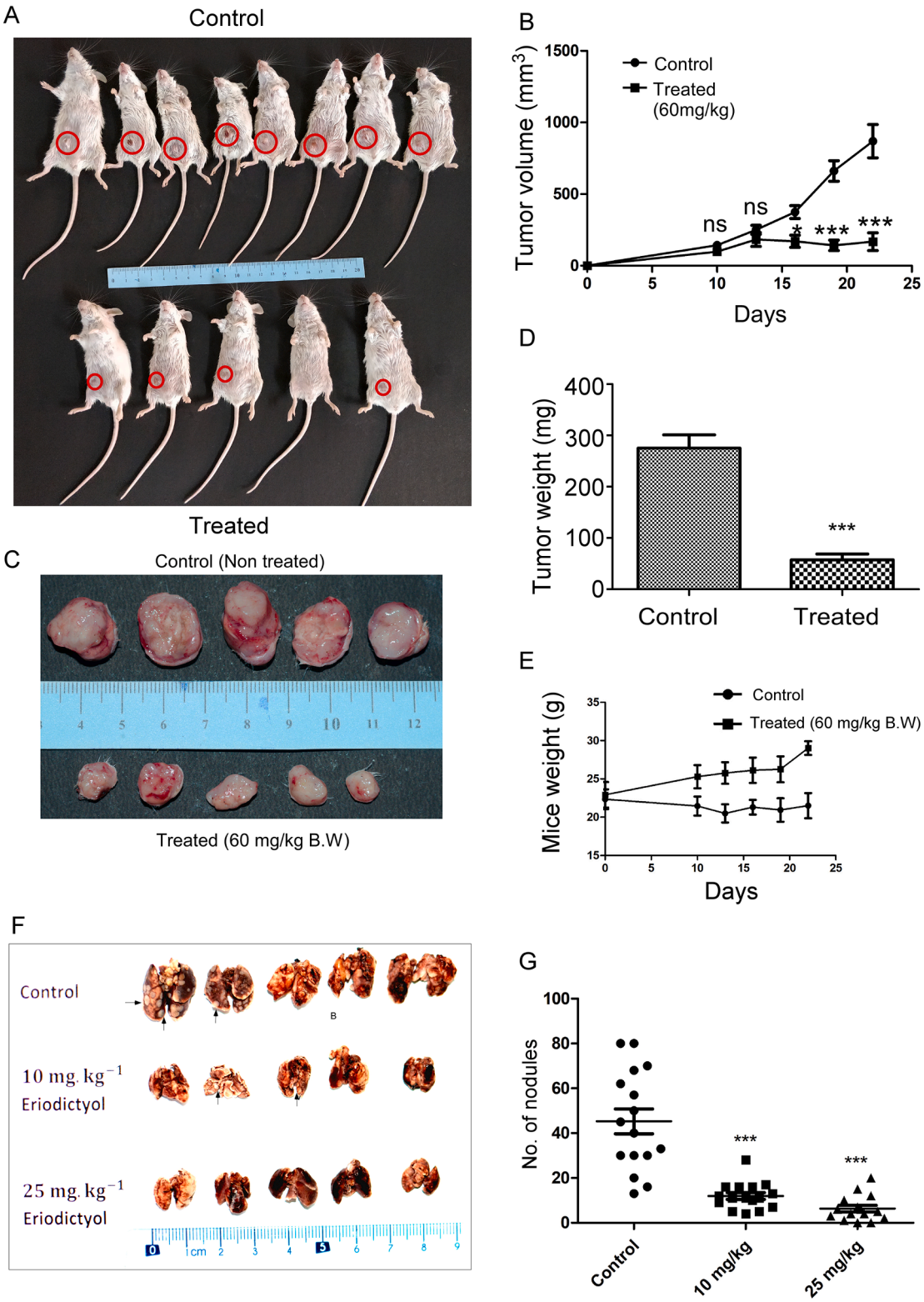

Fig. 9. Eriodictyol impedes the progression of mammary tumors and lung nodules in a syngeneic mouse model. A. Image of mice bearing tumors (indicated by red circles) before sacrifice, injected in the mammary fat pads subcutaneously with 4T1 cells, either treated with Eriodictyol (bottom row) or non-treated (top row). **B.** Line graph showing regression of tumor volume (time-dependent) in response to intraperitoneal injection of Eriodictyol, in Balb/c mice injected subcutaneously with 4T1 cells at the mammary fat pads, in comparison with those non-treated. **C.** Represents image of resected tumors from mice injected in the mammary fat pads subcutaneously with 4T1 cells, either treated with Eriodictyol (bottom row) or non-treated (top row). **D.** Bar graph showing significant reduction in tumor weight of the resected tumors, post-Eriodictyol treatment at 60 mg/kg body weight. **E.** Comparison of mice body weight in eriodictyol-treated vs non-treated. **F.** Photomicrographs depicting formalin-fixed whole lungs from male Balb/c mice injected with 4T1 cells (tail vein injection) with or without Eriodictyol treatment at different concentrations (0, 10, 25 mg/kg body weight). **G.** Graphical representation of the total number of lung nodules counted at different doses (0, 10, 25 mg/kg body weight) of Eriodictyol. The data represents two independent experiments and bar graph represents mean ± SEM (Student's t-test (two-tailed),*$p < 0.05$, **$p < 0.01$, ***$p < 0.001$, ns not significant).

elucidate the comprehensive mechanism of its anti-cancer activity and selectivity towards cancer cells.

TNF family members are the multifunctional cytokines involved in a broad spectrum of biological processes, which includes cell proliferation, cell death, carcinogenesis, immune responses, etc. [26,27]. Binding of TNF ligands to TNF receptors on the cancer cells has been documented to activate the extrinsic apoptosis pathway [28,29], thereby, instigating the initiation of the clinical trials to evaluate the anti-cancer efficacy of rhTNF-α on advanced solid cancers [3,4]. Unfortunately, in contrast to the preclinical studies, the outcome of the clinical trials was disappointing, as evidenced by the decline in apoptosis triggering ability of rhTNF-α, which has been attributed to the simultaneous activation of downstream NF-κB survival pathway [30–32]. Based on these findings, it was inferred that the TNF-α mediated killing of malignant cells through the cell death-receptor pathway could be augmented upon concomitant blockade of NF-κB cascade [33,34]. Since, Eriodictyol activates the downstream signaling that inhibits NF-κB [35,36], we have examined whether inhibition of the same could activate the endogenous TNF-α mediated apoptosis pathway in cancer cells [37]. Previously, some reports have suggested the anti-cancer activity of Eriodictyol on different malignant cells as well as its selectivity towards cancer cells [10,11,38–40]. Nonetheless, the mechanism behind its selective targeting of cancer cells is not yet well-reported, thus, motivating us to understand the underlying mechanism of its selectivity towards cancer cells over normal cells and decipher the precise pathway of Eriodictyol-induced cancer cell death. Here, we have hypothesized that the ability of Eriodictyol to specifically target aberrations contributing to the tumor's proliferative advantage, while sparing normal cells, can lead to a favorable outcome. Our research presents a global as well as differential regulation of gene expression profile in response to Eriodictyol. Among the several biological processes studied, Eriodictyol treatment demonstrated upregulation of a variety of pro-apoptotic and tumor-suppressor genes as well as induction of cell death, confirming its involvement in suppression of tumor cell proliferation. Taken together, our findings offer new possibilities to Eriodictyol's hitherto unrecognized role and unknown mode of action in altering gene transcription as well as unfolding its previously undiscovered anti-cancer characteristics.

Interestingly, our investigation manifests that Eriodictyol-mediated TNFR1 upregulation and releasing of endogenous TNF-α from cancer cells (HeLa), collectively have the fortuitous effect of altering the functional state of the TNF-α pathway from NF-kB dependent cell survival to death-inducing complex formation. In addition, the importance of TNFR1 in Eriodictyol-induced apoptosis is further supported by the exclusive expression of TNFR1 on cancer cells (and not normal cells), wherein Eriodictyol is unable to induce any appreciable TNFR1 expression in normal cells even after prolonged exposure. Additionally, TNFR1 knockout causes significant abrogation of cancer cell apoptosis. Thus, this study uncovers the mechanism behind the selectivity of Eriodictyol-mediated cytotoxic phenomena in cancer cells over normal cells.

Further investigation of the mechanistic details reveals that Eriodictyol induces extrinsic pathways of apoptosis in cancer cells, as evident from the expression profile of hallmark apoptosis-related proteins, which is similar to several previously reported anti-cancer agents [16,41–46]. TNFR1-DISC-Casp-PARP1 is the major axis in the extrinsic apoptosis pathway and we are the first to report the involvement of this pathway in Eriodictyol-mediated selective cytotoxicity in cancer cells. The approach of selectively targeting the extrinsic route to induce apoptosis in tumor cells, such as through ligation of death receptors, is appealing for cancer therapy, since death receptors have a direct link to the cell's death machinery [47]. Furthermore, tumor cell apoptosis has often been shown to occur independently of the p53 tumor suppressor gene, which is lost or inactivated in more than half of human malignancies [48]. PARP-1 cleavage is a crucial event that drives death receptor signaling towards apoptosis or necrosis. TNF-induced oxidative stress and DNA damage activate PARP-1, causing ATP depletion and the subsequent production of necrosis [49]. In brief, we demonstrate that Eriodictyol exposure of the cancer cells causes time-dependent upregulation of endogenous TNF-α and TNFR1 receptor as well as an increase in expression of the DISC complex components (TNFR1, FADD, and TRADD), leading to activation of cleaved caspase 8, activation of effector caspase 7, thus, ultimately resulting in caspases-dependent apoptotic cell death of the cancer cells. Notably, previous studies have already shown TNFR1-induced, however caspase-independent mode of cell death [50,51]. However, the fact that a pan-caspase inhibitor could not completely block Eriodictyol-induced cell death, hints towards a TNFR1-dependent, yet caspase-independent function of Eriodictyol in the induction of cancer cell death. In addition, Eriodictyol-induced apoptosis is accompanied by cell cycle arrest at the G2/M phase, which is initiated by an increase of γ-H2AX (an indicator of DNA damage) through regulation of Cyclin-B1, Cdc25 and Cdc2. Interestingly, Eriodictyol mediated inhibition of Cdc2 leads to accumulation of cells at the G2M phase , thus, resulting in the accumulation of Cyclin B1. Surprisingly, Eriodictyol causes dramatic inhibition of p21. Some reports suggest p21 promotes carcinogenesis and tumor development by promoting transcription of proteins with mitogenic and anti-apoptotic properties [52–54]. Eriodictyol also inactivates Claspin in cancer cells, which plays a vital role in shifting the tumor cell response from cell cycle arrest to induction of apoptotic cell death in response to prolonged DNA replication arrest or the persistence of DNA damage [55,56]. Finally, assessment of the therapeutic efficacy of Eriodictyol in Balb/c (syngeneic) mouse tumor model, subcutaneously injected with 4T1 mice breast cancer cells, indicates that Eriodictyol treatment results in remarkable regression of tumor volume, tumor weight, and metastatic potential in an *in vivo* mouse model without any significant adverse effect on animals as confirmed by body weight difference in untreated vs treated mice.

In the present study, we have elucidated the selective anti-cancer mechanism of Eriodictyol through upregulation of TNFR1 along with G2/M arrest and subsequent, activation of apoptosis in cancer cells without affecting the normal cells. Although the mechanism underlying the Eriodictyol-induced upregulation of TNFR1 in cancer cells is still not clearly understood, the preliminary bioinformatics analysis has shown that several probable TFs as critical targets (data not shown). However, investigation of this phenomenon is beyond the scope of the present study and will be focused on in future research. Although natural plant-based compounds including flavonoids have numerous pharmacological benefits, their large-scale extraction from natural sources in high-purity and consistent form, bioavailability, targeted delivery to the site of interest, toxicity and safety are some of the major challenges in medicinal chemistry. Hence, globally, these compounds are under extensive research as important scaffolds and lead for the development of effective and selective chemotherapeutic agents for clinical application. Henceforth, Eriodictyol might necessitate the development of easy to synthesize (biosynthesis using yeast applying promoter adjustment and directed evolution [57]) and non-toxic chemical derivative, designing strategies to improve its bioavailability by increasing absorption and metabolic stability, as well as its targeted delivery by formulating appropriate microencapsulation, nano-delivery system or micro-emulsion [58–63] for improved anti-cancer strategies. To summarize, Eriodictyol has the capability to be a promising lead for the future development of prospective and efficient candidate for successful cancer therapy.

Fig. 10. Depicts the proposed model of Eriodictyol mediated selective cytotoxicity in cancer cells.

Funding

DBT-Twinning Project (BT/469/NE/TBP/2013), UGC (201314/NETJRF/10501/22 -351787). We acknowledge DST-SERB (Sanction no. EMR/2016/001983) for procurement of the QuantStudio 3 Real Time PCR system, as well as ICMR (Sanction No. 2016-0137/CMB/ADHOC/

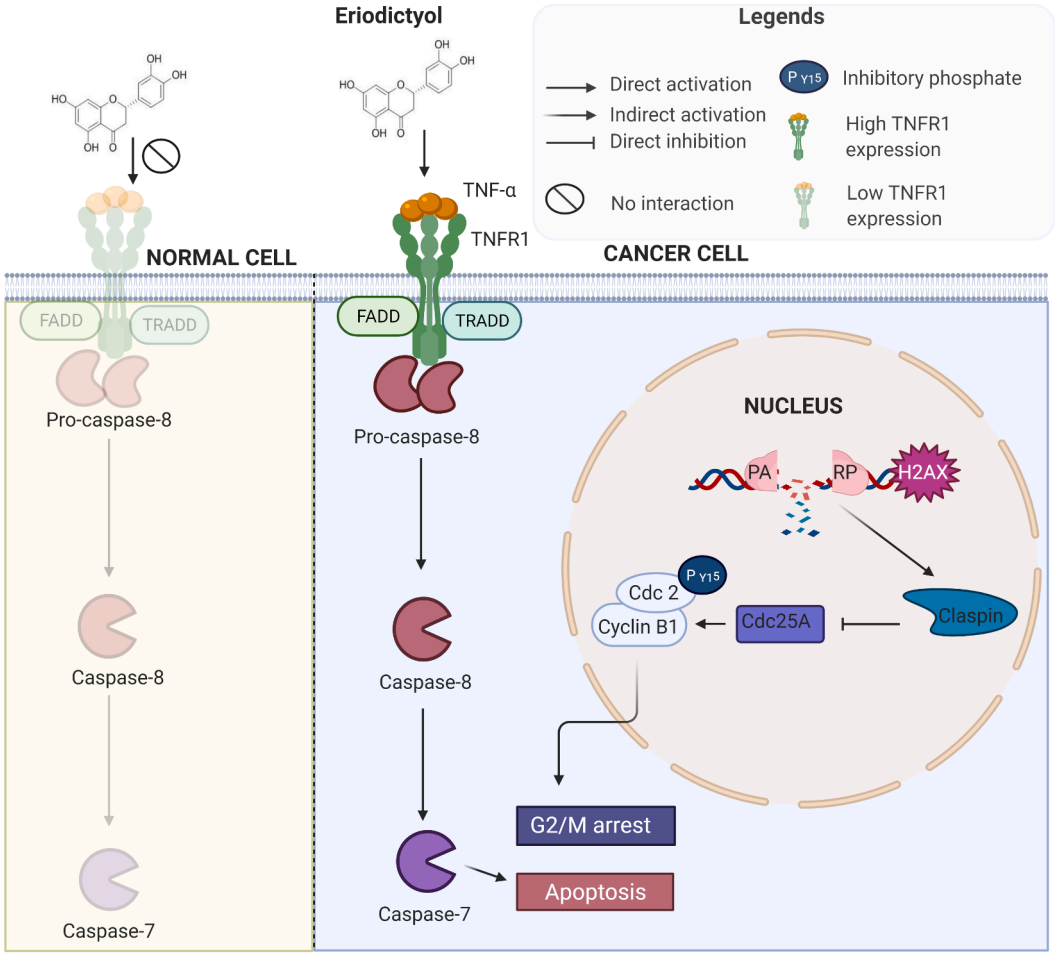

Fig. 10. Proposed model of the role of Eriodictyol mediated selective cytotoxicity of cancer cells. The upregulated expression of TNFR1 on cancer cells lead to Eriodictyol mediated apoptosis.

BMS) for the Gel Imaging System used in this study. Dr. Dipanwita Das Mukherjee is thankful to DBT – Research Associateship (Project ID – P-1453) program in Life Science and Biotechnology, as well as DST-SERB NPDF (Sanction No. PDF/2021/000504) for the post-doctoral fellowships.

Declaration of Competing Interest statement

The authors declare that there is no conflict of interest.

Acknowledgments

We would like to thank BioBharati LifeScience Pvt. Limited for the characterization of TNFR1 KO-6 clones, Dr. Debajyoti Ray for photography of the mice tumors and Mr. Mrinal Das for DNA sequencing. Illustration (Fig. 10) created with https://biorender.com/.

Supplementary materials

Supplementary material associated with this article can be found, in the online version, at doi:10.1016/j.tranon.2022.101433.

References

[1] S. Fulda, Tumor resistance to apoptosis, Int. J. Cancer 124 (3) (2009) 511–515.
[2] R.M. Mohammad, et al., Broad targeting of resistance to apoptosis in cancer, Seminars Cancer Biol. 35 (Suppl(0)) (2015) S78–S103.
[3] T. Mashima, et al., Apoptosis resistance in tumor cells, Cytotechnology 27 (1-3) (1998) 293–308.
[4] D. Tewari, P. Rawat, P.K. Singh, Adverse drug reactions of anticancer drugs derived from natural sources, Food Chem. Toxicol. 123 (2019) 522–535.
[5] Z.-B. Liu, et al., Natural substances derived from herbs or plants are promising sources of anticancer agents against colorectal cancer via triggering apoptosis, J. Pharm. Pharmacol. (2021) rgab130.
[6] X. Ma, Z. Wang, Anticancer drug discovery in the future: an evolutionary perspective, Drug Discovery Today 14 (23) (2009) 1136–1142.
[7] J.K. Lee, Anti-inflammatory effects of eriodictyol in lipopolysaccharide-stimulated raw 264.7 murine macrophages, Arch. Pharm Res. 34 (4) (2011) 671–679.
[8] K. Liu, et al., Eriodictyol inhibits RSK2-ATF1 signaling and suppresses EGF-induced neoplastic cell transformation, J. Biol. Chem. 286 (3) (2011) 2057–2066.
[9] M. Kumazoe, et al., Metabolic profiling-based data-mining for an effective chemical combination to induce apoptosis of cancer cells, Sci Rep 5 (2015) 9474.
[10] L. Tang, et al., Eriodictyol inhibits the growth of CNE1 human nasopharyngeal cancer growth by targeting MEK/ERK signalling pathway, inducing cellular autophagy and inhibition of cell migration and invasion, J. BUON 25 (5) (2020) 2389–2394.
[11] Y. Zhang, R. Zhang, H. Ni, Eriodictyol exerts potent anticancer activity against A549 human lung cancer cell line by inducing mitochondrial-mediated apoptosis, G2/M cell cycle arrest and inhibition of m-TOR/PI3K/Akt signalling pathway, Arch. Med. Sci. 16 (2) (2019) 446–452.
[12] Li, W., et al., *Eriodictyol Inhibits Proliferation, Metastasis and Induces Apoptosis of Glioma Cells via PI3K/Akt/NF-κB Signaling Pathway.*2020. 11(114).
[13] M. Kundu, et al., Ganglioside GM2 mediates migration of tumor cells by interacting with integrin and modulating the downstream signaling pathway, Biochimica et Biophysica Acta (BBA) - Molecular Cell Res. 1863 (7, Part A) (2016) 1472–1489.
[14] J. van Meerloo, G.J. Kaspers, J. Cloos, Cell sensitivity assays: the MTT assay, Methods Mol. Biol. 731 (2011) 237–245.
[15] A. Dutta, et al., C-Glycosylated cinnamoylfuran derivatives as novel anti-cancer agents, RSC Adv. 7 (46) (2017) 28853–28864.
[16] P.K. Parida, et al., Inhibition of cancer progression by a novel trans-stilbene derivative through disruption of microtubule dynamics, driving G2/M arrest, and p53-dependent apoptosis, Cell Death. Dis. 9 (5) (2018) 448.

[17] M.F. Sentmanat, et al., A survey of validation strategies for CRISPR-Cas9 editing, Sci. Rep. 8 (1) (2018), 888-888.
[18] B. Mahata, et al., TALEN mediated targeted editing of GM2/GD2-synthase gene modulates anchorage independent growth by reducing anoikis resistance in mouse tumor cells, Sci. Rep. 5 (1) (2015) 9048.
[19] R. Minorics, et al., A molecular understanding of D-homoestrone-induced G2/M cell cycle arrest in HeLa human cervical carcinoma cells, J. Cell Mol. Med. 19 (10) (2015) 2365–2374.
[20] H. Rauert, et al., TNFR1 and TNFR2 regulate the extrinsic apoptotic pathway in myeloma cells by multiple mechanisms, Cell Death Dis. 2 (8) (2011) e194.
[21] D. Hanahan, R.A. Weinberg, The hallmarks of cancer, Cell 100 (1) (2000) 57–70.
[22] K. Fernald, M. Kurokawa, Evading apoptosis in cancer, Trends Cell Biol. 23 (12) (2013) 620–633.
[23] F. Guestini, K.M. McNamara, H. Sasano, The use of chemosensitizers to enhance the response to conventional therapy in triple-negative breast cancer patients, Breast Cancer Manage. 6 (4) (2017) 127–131.
[24] A.R. Hamed, et al., Targeting multidrug resistance in cancer by natural chemosensitizers, Bull. Natl. Res. Centre 43 (1) (2019) 8.
[25] J.A. Shabbits, Y. Hu, L.D. Mayer, Tumor chemosensitization strategies based on apoptosis manipulations, Mol Cancer Ther 2 (8) (2003) 805–813.
[26] G.D. Kalliolias, L.B. Ivashkiv, TNF biology, pathogenic mechanisms and emerging therapeutic strategies, Nat. Rev. Rheumatol. 12 (1) (2016) 49–62.
[27] H.T. Idriss, J.H. Naismith, TNF alpha and the TNF receptor superfamily: structure-function relationship(s), Microsc. Res. Tech. 50 (3) (2000) 184–195.
[28] O. Micheau, J. Tschopp, Induction of TNF receptor I-mediated apoptosis via two sequential signaling complexes, Cell 114 (2) (2003) 181–190.
[29] E.E. Varfolomeev, A. Ashkenazi, Tumor necrosis factor: an apoptosis JuNKie? Cell 116 (4) (2004) 491–497.
[30] O. Micheau, et al., NF-κB Signals Induce the Expression of c-FLIP, Mol. Cell. Biol. 21 (16) (2001) 5299–5305.
[31] S.F. Josephs, et al., Unleashing endogenous TNF-alpha as a cancer immunotherapeutic, J. Transl. Med. 16 (1) (2018) 242.
[32] C.G. Savva, et al., Selective activation of TNFR1 and NF-κB inhibition by a novel biyouyanagin analogue promotes apoptosis in acute leukemia cells, BMC Cancer 16 (2016), 279-279.
[33] Y. Wang, et al., Eriodictyol inhibits IL-1β-induced inflammatory response in human osteoarthritis chondrocytes, Biomed. Pharmacother. 107 (2018) 1128–1134.
[34] A. Wicovsky, et al., Sustained JNK activation in response to tumor necrosis factor is mediated by caspases in a cell type-specific manner, J. Biol. Chem. 282 (4) (2007) 2174–2183.
[35] Y. Wang, et al., Eriodictyol inhibits IL-1β-induced inflammatory response in human osteoarthritis chondrocytes, Biomed. Pharmacother. 107 (2018) 1128–1134.
[36] X. Wang, et al., Eriodictyol ameliorates lipopolysaccharide-induced acute lung injury by suppressing the inflammatory COX-2/NLRP3/NF-κB pathway in mice, J Biochem. Mol. Toxicol. 34 (3) (2020) e22434.
[37] W. Li, et al., Eriodictyol inhibits proliferation, metastasis and induces apoptosis of glioma Cells via PI3K/Akt/NF-κB signaling pathway, Front. Pharmacol. 11 (2020) 114.
[38] K. Liu, et al., Eriodictyol inhibits RSK2-ATF1 signaling and suppresses EGF-induced neoplastic cell transformation, J. Biol. Chem. 286 (3) (2011) 2057–2066.
[39] M. Kumazoe, et al., Metabolic Profiling-based Data-mining for an Effective Chemical Combination to Induce Apoptosis of Cancer Cells, Sci. Rep. 5 (1) (2015) 9474.
[40] W. Li, et al., Eriodictyol inhibits proliferation, metastasis and induces apoptosis of glioma Cells via PI3K/Akt/NF-κB signaling pathway, Front. Pharmacol. 11 (114) (2020).
[41] B. Mahata, et al., GBM derived gangliosides induce T cell apoptosis through activation of the caspase cascade involving both the extrinsic and the intrinsic pathway, PLoS One 10 (7) (2015), e0134425.
[42] L. Belayachi, et al., Retama monosperma n-hexane extract induces cell cycle arrest and extrinsic pathway-dependent apoptosis in Jurkat cells, BMC Complement. Alternative Med. 14 (2014), 38-38.
[43] S.H. Park, et al., Luteolin induces cell cycle arrest and apoptosis through extrinsic and intrinsic signaling pathways in MCF-7 breast cancer cells, J. Environ. Pathol. Toxicol. Oncol. 33 (3) (2014) 219–231.
[44] B. Wang, X.H. Zhao, Apigenin induces both intrinsic and extrinsic pathways of apoptosis in human colon carcinoma HCT-116 cells, Oncol. Rep. 37 (2) (2017) 1132–1140.
[45] H. Wahl, et al., Curcumin enhances Apo2L/TRAIL-induced apoptosis in chemoresistant ovarian cancer cells, Gynecol. Oncol. 105 (1) (2007) 104–112.
[46] A. Chopra, A. Anderson, C. Giardina, Novel piperazine-based compounds inhibit microtubule dynamics and sensitize colon cancer cells to tumor necrosis factor-induced apoptosis, J. Biol. Chem. 289 (5) (2014) 2978–2991.
[47] A. Ashkenazi, Targeting death and decoy receptors of the tumour-necrosis factor superfamily, Nat. Rev. Cancer 2 (6) (2002) 420–430.
[48] W.S. El-Deiry, Insights into cancer therapeutic design based on p53 and TRAIL receptor signaling, Cell Death Differ. 8 (11) (2001) 1066–1075.
[49] Los, M., et al., *Activation and Caspase-mediated Inhibition of PARP: a molecular switch between fibroblast necrosis and apoptosis in death receptor signaling.*2002. 13(3): p. 978-988.
[50] J. Li, et al., Beta-actin is required for mitochondria clustering and ROS generation in TNF-induced, caspase-independent cell death, J. Cell Sci. 117 (Pt 20) (2004) 4673–4680.
[51] M.J. Morgan, Y.-S. Kim, Z.-g. Liu, TNFα and reactive oxygen species in necrotic cell death, Cell Res. 18 (3) (2008) 343–349.
[52] R.U. Jänicke, et al., The multiple battles fought by anti-apoptotic p21, Cell Cycle 6 (4) (2007) 407–413.
[53] L. Lai, G.Y. Shin, H. Qiu, The role of cell cycle regulators in cell survival-dual functions of cyclin-dependent kinase 20 and p21(Cip1/Waf1), Int. J. Mol Sci. 21 (22) (2020).
[54] I.B. Roninson, Oncogenic functions of tumour suppressor p21(Waf1/Cip1/Sdi1): association with cell senescence and tumour-promoting activities of stromal fibroblasts, Cancer Lett. 179 (1) (2002) 1–14.
[55] J.I. Semple, et al., Cleavage and degradation of Claspin during apoptosis by caspases and the proteasome, Cell Death & Different. 14 (8) (2007) 1433–1442.
[56] C.A. Clarke, L.N. Bennett, P.R. Clarke, Cleavage of claspin by caspase-7 during apoptosis inhibits the Chk1 pathway, J. Biol. Chem. 280 (42) (2005) 35337–35345.
[57] S. Gao, et al., Efficient Biosynthesis of (2S)-Eriodictyol from (2S)-Naringenin in Saccharomyces cerevisiae through a Combination of Promoter Adjustment and Directed Evolution, ACS Synthetic Biol. 9 (12) (2020) 3288–3297.
[58] Q. Shen, et al., Enhanced intestinal absorption of daidzein by borneol/menthol eutectic mixture and microemulsion, AAPS PharmSciTech 12 (4) (2011) 1044–1049.
[59] T. Walle, Methylation of dietary flavones greatly improves their hepatic metabolic stability and intestinal absorption, Mol. Pharmaceutics 4 (6) (2007) 826–832.
[60] H. Cao, et al., Methylation of genistein and kaempferol improves their affinities for proteins, Int. J. Food Sci. Nutr. 64 (4) (2013) 437–443.
[61] I.L. Nielsen, et al., Bioavailability is improved by enzymatic modification of the citrus flavonoid hesperidin in humans: a randomized, double-blind, crossover trial, J. Nutr. 136 (2) (2006) 404–408.
[62] D.J. Bharali, et al., Nanoparticle delivery of natural products in the prevention and treatment of cancers: current status and future prospects, Cancers 3 (4) (2011) 4024–4045.
[63] J.K. Patra, et al., Nano based drug delivery systems: recent developments and future prospects, J. Nanobiotechnol. 16 (1) (2018) 71.